## Special Feature: Sensors

*Research Report*

# An SOI MEMS 3-axis Accelerometer with a Zigzag-shaped Z-electrode for Fully Differential Detection

Motohiro Fujiyoshi, Yutaka Nonomura, Hirofumi Funabashi, Yoshiteru Omura, Teruhisa Akashi, Yoshiyuki Hata and Masayoshi Esashi

*Report received on May 27, 2014*

**ABSTRACT** For advanced motion control of automobiles and robots, we have developed a fully-differential 3-axis accelerometer by using micro electro mechanical systems (MEMS) technology. We used the following four approaches to achieve a high-accuracy 3-axis accelerometer: (1) Single-crystal silicon was chosen as the sensor material to increase reliability for automobile use. (2) To improve sensor accuracy, a zigzag-shaped electrode (ZSZ) structure was proposed. The ZSZ enabled differential detection in the Z direction by two capacitors with only two conductive layers, and the gaps of the ZSZ were equal because different sections of the same oxide layer of an SOI wafer was used in both. (3) To reduce cross sensitivity, translational motions of mass were achieved by the combination of straight and folded beams for springs. (4) A chip-level warp control was proposed. Warp control was performed by forming a $SiO_2$ frame on the back side of the chip. The $SiO_2$ frame worked as a stress compensator of thermal expansion, and the gaps of the ZSZ were controlled to be precisely equal.

The experimental results for a prototype 3-axis accelerometer showed low cross-axis sensitivity and non-linearity: a cross-axis sensitivity of Z-axis outputs before differential amplification as small as 1.4% FS (FS = +/–1.5g) and a non-linearity of 0.4% FS.

**KEYWORDS** SOI, 3-axis, Accelerometer, Differential Detection, Zigzag-shaped Z-electrode, MEMS Sensor, Warp Control

## 1. Introduction

Demand for accelerometers for use in automobiles is increasing. Anti-lock braking systems (ABS) and vehicle stability control systems (VSC) have been developed as pre-crash safety features. Accelerometers are used in these systems along with angular-rate, speed, and steering wheel position sensors. The most important characteristics of accelerometers for such purposes are sensor accuracy and reliability. Automobiles are exposed to a wide range of temperatures, including severe cold and heat. Therefore, a highly stabilization of zero output is required, because the zero output indicates the initial attitude and dynamic state of the body. Furthermore, automobiles are typically used for a long time, often for more than ten years. Therefore, automotive accelerometers should operate without failure for more than a decade.

Next-generation advanced automotive control systems that consider the attitude of the vehicle will provide an extra margin of safety. Current automobiles are assumed to move on a flat road, perpendicular to the Earth's gravity. Therefore, only one- or two-axis accelerometers that detect horizontal acceleration have been used. However, the attitude of the vehicle will change with any slope of the road's surface or deformation of the automobile's suspension. Therefore, high-precision three-axis accelerometers should be required, such as those used for robot motion control systems.

In this paper, we report the development of a fully differential three-axis accelerometer using micro electromechanical systems (MEMS) technology. We discuss the key challenges in the realization of a precise three-axis accelerometer based on MEMS technology.

## 2. Problems in Developing a Precise 3-axis Accelerometer

MEMS technology is widely applied in many sensors, such as accelerometers and gyroscopes. To detect the displacement of a mass and/or beam by inertial force, there are three detection methods available: the piezoresistive method, which uses resistance variation

 

due to strain in the beams; the piezoelectric method, which uses the electromotive force generated by strain in the beams; and the capacitive detection method, which uses capacitance variation caused by changes in the width of a gap between two electrodes. The capacitive detection method is useful for MEMS sensors. There are many reasons for this. The capacitance between two electrodes is stable over a wide temperature range as long as the width of the gap between the two electrodes remains constant. Furthermore, the electrodes are suitable for miniaturization by MEMS technology. Finally, the capacitive detection method is capable of static gap measurement.

When selecting a capacitive detection method, a differential method offers improved accuracy and sensor output stability. Furthermore, a fully differential detection method has many advantages such as the elimination of parasitic capacitance, reduction of cross-axis sensitivity and non-linearity, and stabilization of zero output under temperature variation. However, it is difficult to apply a fully differential method to detection along the z-axis because of the following two problems.

First, the two electrodes must be placed on either side of the seismic mass with exactly the same gap widths for precise detection of mass movement. The gaps for z-electrodes are generally made using two different sacrificial layers in MEMS technology. However, it is difficult to deposit two layers that are precisely the same thickness because of the slight inherent non-uniformity of film deposition and etching depth.[1,2] A differential z-electrode-type sensor composed of multiple layers of CMOS interconnection metals has been reported.[3] However, it is difficult to match the gaps due to residual stress in the metal layers.

As a stable material, silicon on insulator (SOI) wafers are often used in automotive sensors.[4] The structures of our sensors generally had planar symmetry in order to maintain strain balance in the device structure over a wide temperature range. However, the vertical structures along the z-axis were not symmetrical, so stress and warpage in the devices produced dimensional changes in the z-electrode after processing and with variations in temperature.

Second, the mass should move perpendicularly to the electrode surfaces. However, commercial MEMS three-axis accelerometers detect acceleration by rotary motion instead of the translational motion of a mass.[5,6] Because cross contamination occurs between rotary and translational motion of the mass, it is difficult to precisely separate the sensor outputs into their components along each axis. As a consequence, the cross-axis sensitivities of the sensors are degraded.

We propose a novel structure that can detect mass displacement with precise differential electrodes. There are four challenges: selection of stable materials, accurate displacement detection of the seismic mass along the z-axis, reduction of cross talk sensitivity for the three-axis accelerometer, and significant improvement of the accuracy. These challenges, labeled A through D, and their solutions, are discussed below.

## 3. Challenges and Solutions

### 3. 1 Materials for Sensor Structure (A)

For accelerometers in automobiles, the sensor materials should have stable characteristics over a wide temperature range, low warpage during fabrication, and durable long-term spring constants.

Unlike polycrystalline silicon made by chemical vapor deposition (CVD) and plated metals, single-crystal silicon has no grains and no stress distribution. The physical properties of monocrystalline silicon such as the Young's modulus and thermal expansion coefficient are stable during fabrication and show reproducible values. There appear to be no fatigue effects in single-crystal silicon, even after long-term vibration. For these reasons, single-crystal silicon has excellent spring characteristics for sensor beams and structures. An SOI wafer composed of single-crystal silicon and silicon oxide was selected as the sensor material.

### 3. 2 ZSZ Electrodes with Equal Gaps (B)

It is difficult to form equal gaps in a differential detection structure. A basic differential detection method is shown in **Fig. 1**. This structure requires three conductive layers, labeled 1 to 3 in the figure. Conductive layer 2 is a seismic mass for an accelerometer. Conductive layers 1 and 3 face conductive layer 2 to form two capacitors, *C1* and *C2*. When layer 2 moves toward layer 3 by a distance $\Delta z$ in the z-direction due to an inertial force, gap 1 will widen and gap 2 will narrow. As a result, the capacitance of *C1* will decrease and that of *C2* will increase. In our

 

experiments, which employed the differential detection method given by Eq. (1), the differential output $C2 - C1$ was obtained using C-V conversion circuits.

$$\Delta C = C2 - C1 = \varepsilon_0 \cdot S \cdot \left( \frac{1}{d_0 - \Delta z} - \frac{1}{d_0 + \Delta z} \right) \quad (1)$$

where $\varepsilon_0$ is the permittivity of free space, $S$ is the electrode area, $d_0$ is the initial gap, and $\Delta z$ is the z-displacement of conductive layer 2.

However, the SOI wafer has only two conductive layers. To overcome this problem, we proposed the zigzag-shaped z-electrode (ZSZ) structure shown in **Fig. 2**. Conductive layers 1 and 2 are divided and electrically connected to each other. These connected conductive layers act as a seismic mass. The other parts of layers 1 and 2 act as upper and lower electrodes. Capacitors *C1* and *C2* are formed between the seismic mass and layers 1 and 2, respectively. When the seismic mass moves in the z-direction, *C1* and *C2* vary inversely in proportion to the displacement, as shown in Fig. 1.

An actual sensor structure is shown in **Fig. 3**(a).

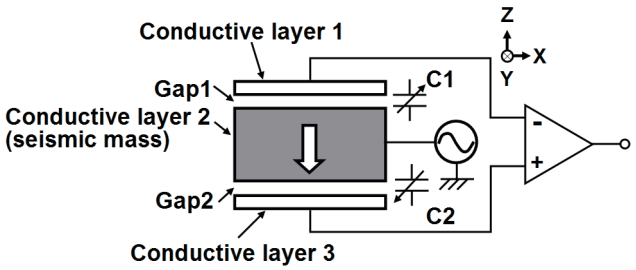


**Fig. 1** Basic differential detection method.

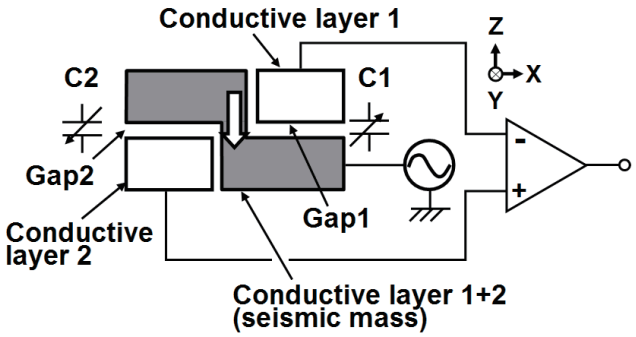


**Fig. 2** Differential detection method using a zigzag-shaped z-electrode (ZSZ) structure.

The upper Si layer of the SOI is used for the upper electrodes, and the lower Si layer of the SOI is used for the lower electrodes. The electrodes of the upper and lower Si layers are divided by grooves and electrically isolated from the other parts. Part of the upper electrode is electrically connected to the lower electrode via interconnections. After oxide etching, the gaps and movable parts are formed.

The ZSZ structure consists of two kinds of capacitors, *C1* and (*C2* + *C3*). The initial capacitances of *C1* and (*C2* + *C3*) are precisely equal when the overlapping electrode area of *C1* is equal to that of (*C2* + *C3*). This is because all three gaps are determined by the thickness of the same oxide layer of the SOI wafer.

When an acceleration is applied in the z-axis direction, the seismic mass moves in the z-direction, as shown in Fig. 3(b), and the capacitances of *C1* and (*C2* + *C3*) change. When the capacitance of *C1* decreases, that of (*C2* + *C3*) increases. By measuring the difference between the capacitances of *C1* and (*C2* + *C3*), the mass displacement in the z-direction can be precisely determined.

### 3. 3 Translational Motion of the Mass (C)

In Fig. 3(b), the differential detection method works effectively when the seismic mass moves in translational modes. Therefore, a combination of two different types of beams (folded and straight) was used to intensify the anisotropy of the vibrational directions.

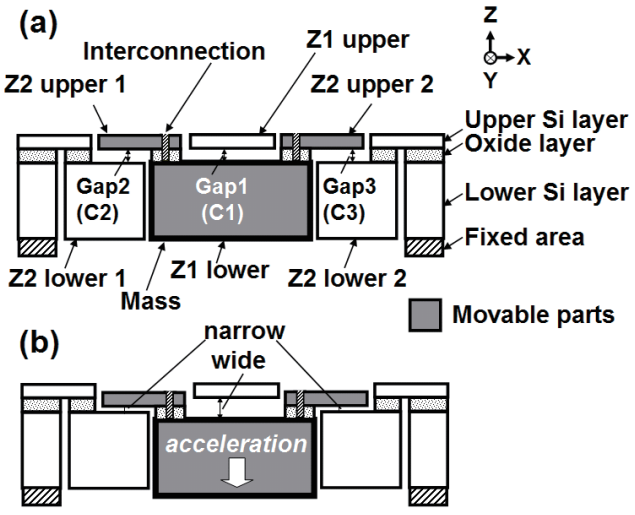


**Fig. 3** ZSZ sensor structure with three gaps: (a) with no acceleration, (b) with acceleration in the z-direction.

The ZSZ structure and a combination of beam types were applied to construct a fully differential three-axis accelerometer. Top and cross-sectional views of the sensor are shown in **Figs. 4**(a) and (b). The beams have highly independent bending directions, and the combination of beams prevents mass rotation. This design reduces cross-axis sensitivity.[4]

The straight beams connected to the mass are also connected perpendicularly to the folded beams. The combination of the two beams releases the internal stress of the straight beams and maintains a stable stiffness under temperature variations.

The ZSZ structure is placed in the middle of the sensor. The movable parts are supported by four straight beams and four folded beams. The spring stiffness in the z-direction depends on the sum of the z-direction stiffness of the X, Z and Y, Z beams.

B-B and C-C cross-sectional views of the ZSZ structure are shown in **Fig. 5**. The Z2 lower electrode is supported by the upper Si with an oxide layer and faces the Z2 upper electrode. The Z1 upper electrode is located on the lower Si layer with the oxide layer and faces the Z1 lower electrode. The gaps between the Z1 upper and lower electrodes and between the Z2 upper and lower electrodes are the same because they straddle the same oxide layer.

Comb-shaped X-electrodes are connected to both sides of the moving parts, and Y-electrodes are connected to the connector. The capacitances of X1 and X2 vary inversely in response to x-displacement of the moving parts. The capacitances of Y1 and Y2 vary inversely in response to y-displacement of the connecting parts. All displacements of the moving parts are detected by this fully differential detection method.

### 3. 4 Reduction of Sensor Chip Warp (D)

The backside shape of the sensor chip is shown in **Fig. 6**, which was obtained using a 3D optical surface profilometer with scanning light interferometry. The sensor chip was warped because of a stress imbalance in the z-direction, which was caused by the removal of all of the backside oxide layer and part of the middle oxide layer. Chip warpage is undesirable, as it can adversely affect sensor performance.

An Si wafer or chip with an oxide layer warps due to internal stresses, such as the thermal stress caused by a difference in coefficients of thermal expansion and residual stresses. The internal stress $\sigma$ of a thin film on a substrate is expressed by Eq (2). Here, the thickness of the substrate is $d$, the radius of curvature is $r$, the Young's modulus is $E$, Poisson's ratio is ν, and the thickness of the thin film is $t$. For a square chip, the internal stress $\sigma$ is given by Eq (3), where $\delta$ is the displacement of the chip by the stress and $l$ is the side length of the square chip.

The model upon which these equations are based is a single thin layer on a single substrate.

$$\sigma = \frac{E \cdot d^2}{6 \cdot r \cdot t\left(1-\nu\right)} \tag{2}$$

$$\sigma = \frac{E \cdot d^2 \cdot \delta}{3 \cdot r \cdot l^2\left(1-\nu\right)} \tag{3}$$

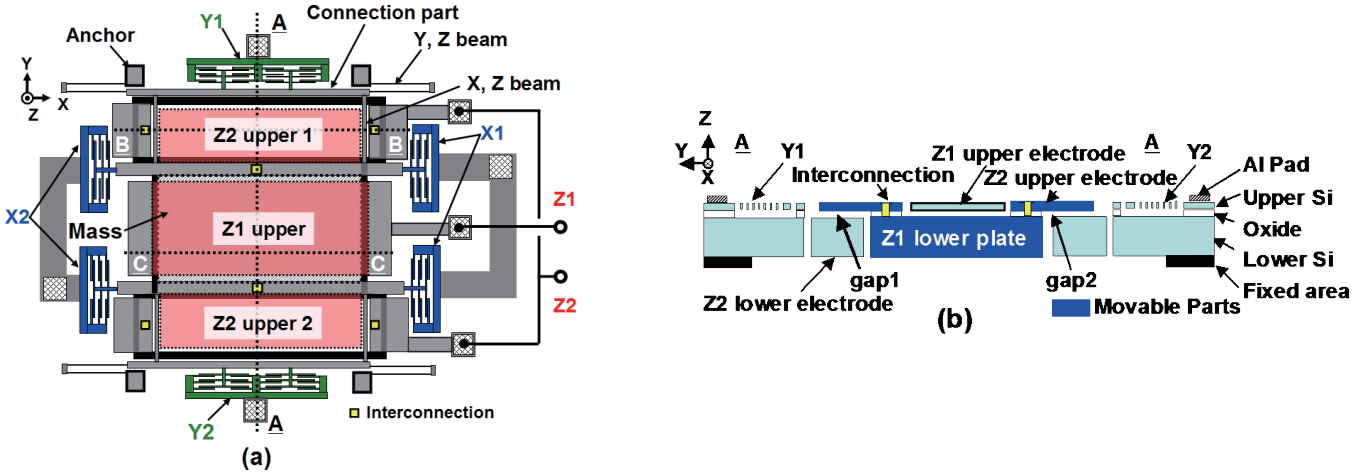


**Fig. 4** Top-view schematic of the 3-axis accelerometer (a), cross-sectional view (b).

The three-axis accelerometer sensor chip consists of three layers; namely, upper Si, buried $SiO_2$, and lower Si. The upper Si and buried $SiO_2$ layers are partially removed from the central area of the chip to form the sensor structure. As it was difficult to analyze this structure using the above equations, the finite element method (FEM) was used to calculate the warpage of the sensor, as shown in **Fig. 7**.

To keep the sensor chip flat, chip-level warp control was performed by forming an $SiO_2$ frame on the back side of the chip. This backside frame acts as a thermal expansion stress compensator.

## 4. Fabrication

The upper Si layer of the SOI wafer was etched by the 1st deep reactive ion etching (DRIE) step to form interconnection holes, and these holes were filled with a conductive material. The upper Si was etched by a 2nd DRIE step to form the upper electrodes. The lower Si layer was etched by a 3rd DRIE to form the lower electrodes. Finally, the oxide sacrificial layer that forms the box layer and the $SiO_2$ on the back side for chip warp control were partially etched by a vapor hydrofluoride (VHF) etching technique to release the movable parts on the chip.

## 5. Results

**Fig. 8** shows a scanning electron microscope (SEM) photograph of the developed three-axis accelerometer. The sensor area was 3 × 3 mm in size. **Fig. 9** shows a backside view of the sensor. The lower Si layer was divided, and the Z1 and Z2 lower electrodes were observed. The developed sensor chip was mounted in a package, as shown in **Fig. 10**.

Evaluation of the sensor characteristics was carried out using the Earth's gravity by rotating the sensor by every 10 degrees step along the x-axis, y-axis, and z-axis. Output signals from each electrode before

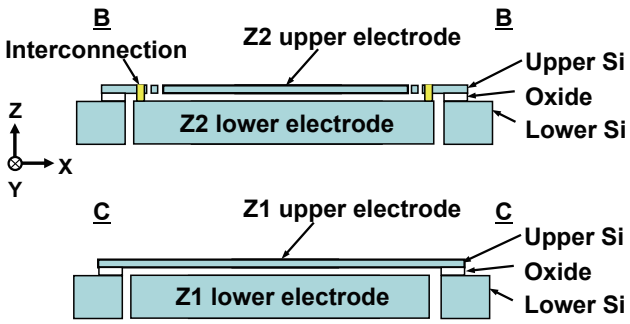


**Fig. 5** Cross sections of the Z1 and Z2 electrodes B-B and C-C in Fig. 4(a).

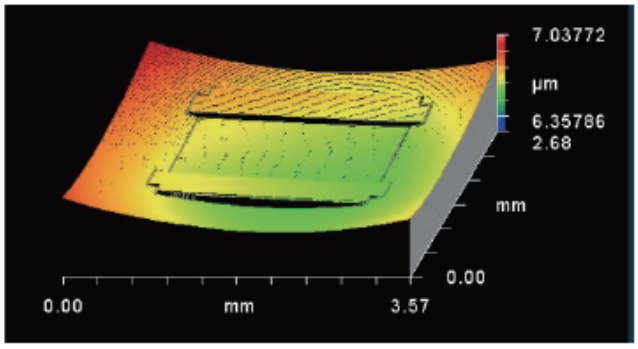


**Fig. 6** 3D optical surface profile of the backside of a sensor chip with no backside frame.

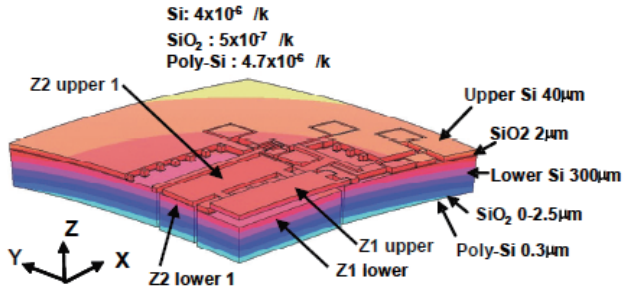


**Fig. 7** FEM analysis results for a 1/4 sensor chip model.

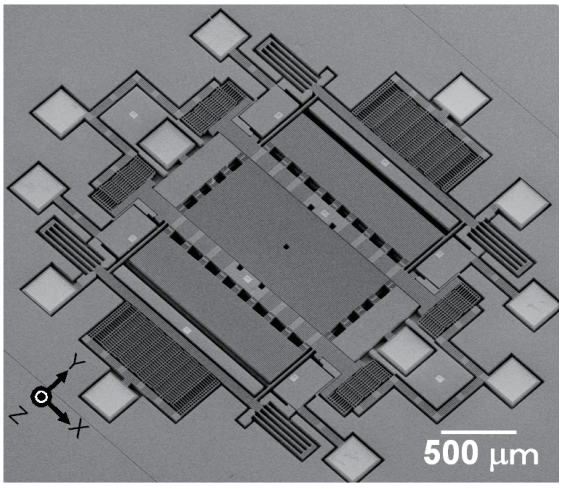


**Fig. 8** SEM photograph of the developed accelerometer.

 

differential amplification are shown in **Fig. 11**. The cross-axis sensitivity of the x-axis outputs before differential amplification was 1.4% FS (FS = +/–1.5g). **Fig. 12** shows the differential sensor outputs. A non-linearity of 0.4% FS was obtained.

The backside $SiO_2$ frame on the sensor chip for stress compensation is shown in **Fig. 13**. The backside frame controlled the warp, and resulted in a good flatness of the sensor chip. A 3D optical surface profile of the backside of a sensor chip is shown in **Fig. 14**. The inverses of the measured and FEM-calculated curvature radii decreased linearly with increasing thickness of the backside frame, as shown in **Fig. 15**.

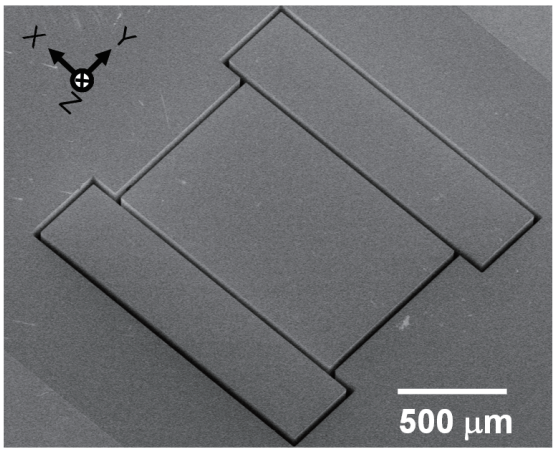


**Fig. 9** Backside view of a sensor without the backside frame.

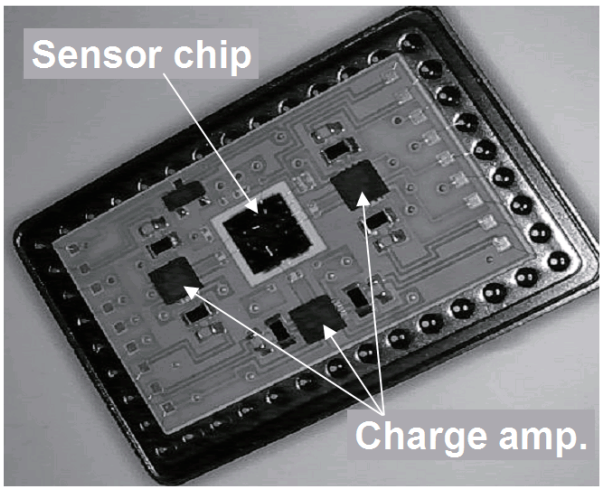


**Fig. 10** Packaged ZSZ 3-axis accelerometer with charge amplifier.

There was a difference in zero points between the measured $Rmea^{-1}$ line and the FEM-calculated $Rfem^{-1}$ line.

The zero point of the measured $Rmea^{-1}$ was T = 2.6 μm of backside frame thickness, but the zero point of the FEM $Rfem^{-1}$ was T = 1.7 μm. Optically measured gap differences between $Gap_{Z1}$ and $Gap_{Z2}$ are also shown in Fig. 15, and these differences decreased linearly with increasing backside frame thickness. The zero point of the optically measured gap difference line

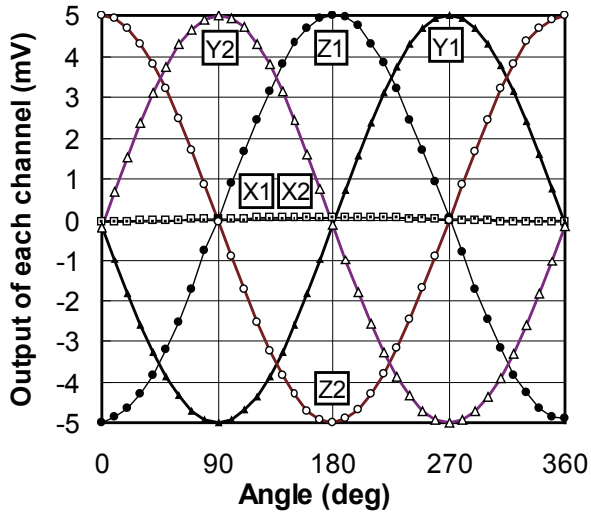


**Fig. 11** Outputs of each channel before differential amplification. Acceleration of gravity was applied to the sensor by rotating the sensor by every 10 degrees step.

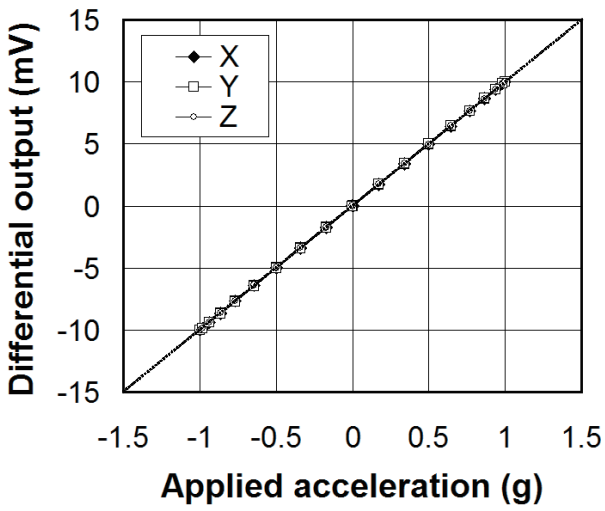


**Fig. 12** Three-axis outputs after differential amplification.

is 3.0 μm. After the evaluation, we determined the cause of the mismatch between the experimental and FEM-calculated results: the original SOI wafers were warped. Usually, as-received SOI wafers exhibit a degree and shape of warpage that is controlled by the wafer manufacturer. Therefore, as-received SOI wafer warpage should be taken into consideration when determining the proper backside frame thickness.

Measured offset and sensitivity ratios are plotted as a function of backside $SiO_2$ thickness in **Fig. 16**. Here, the offset ratio is the ratio of an offset output of the Z2 electrode divided by an offset output of the Z1 electrode. The sensitivity ratio is the ratio of a Z2 electrode output sensitivity divided by a Z1 electrode output sensitivity. The offset and sensitivity ratios rapidly decreased to 1 as the backside frame thickness increased. However, the results shown in Fig. 15 indicate that the offset and sensitivity ratios can be adjusted to 1 by using a backside frame thickness of approximately 2.5 to 3.0 μm. By properly forming the backside frame, the offset outputs and sensitivities in the z-direction can be made almost the same, enabling a high-performance SOI three-axis accelerometer with a ZSZ structure.

## 6. Conclusion

We have developed a fully differential three-axis accelerometer for motion control of automobiles and robots. To increase the performance of the sensor, four solutions, labeled (A) to (D), were developed, as summarized below.

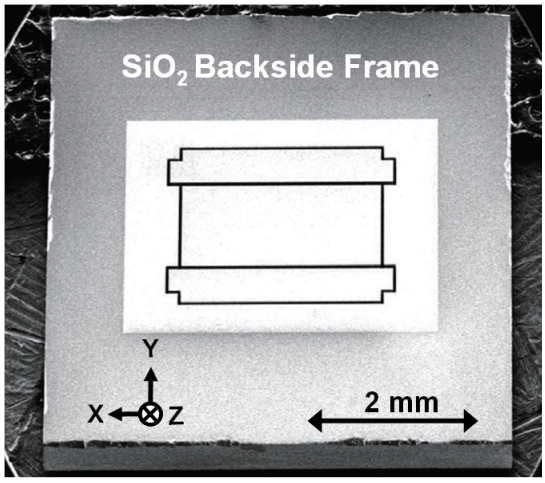


**Fig. 13** Backside view of a sensor with a backside frame.

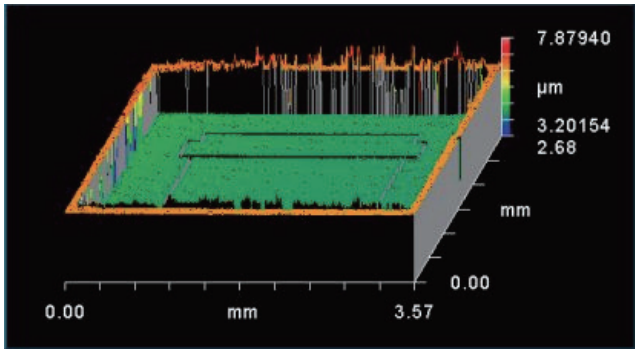


**Fig. 14** 3D optical surface profile of the backside of a sensor chip with a backside frame.

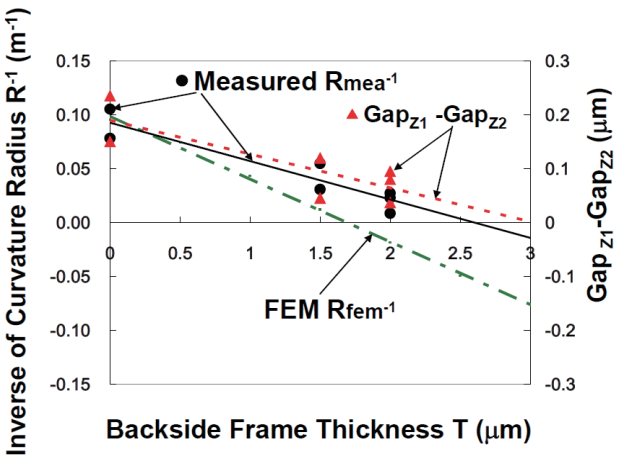


**Fig. 15** Inverse curvature and gap vs. backside frame thickness.

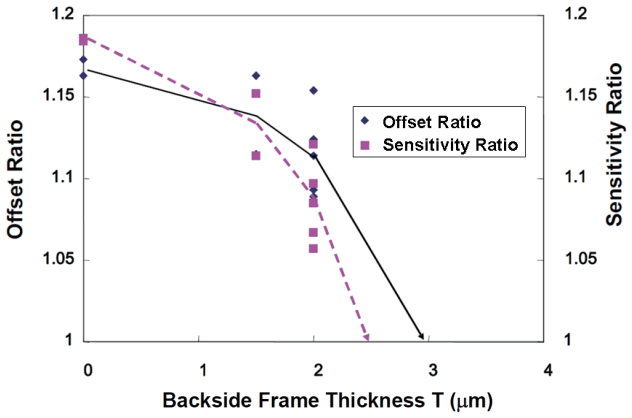


**Fig. 16** Offset and sensitivity ratios vs. frame thickness.

(A) Single crystal silicon was chosen as the sensor material to keep the sensor characteristics stable.

(B) A ZSZ electrode structure with SOI was proposed to obtain equal gap widths for differential detection along the z-axis.

(C) Combinations of beams were designed to enforce translational motion and restrict rotational motion of the sensor's seismic mass to reduce cross-axis sensitivity.

(D) An $SiO_2$ frame on the backside of the chip was formed to control chip-level warpage by compensating for thermal expansion stress.

Experimental results for a prototype sensor chip implementing solutions (A) to (C) demonstrated low cross-axis sensitivity and non-linearity, cross-axis sensitivity of the z-axis outputs before differential amplification as low as 1.4% FS (FS = +/–1.5g), and a non-linearity of 0.4% FS.

However, a small capacitor gap difference in the z-direction appeared, causing unequal sensitivities. We therefore proposed a novel method for chip-level warpage control as solution (D). This chip-level warpage control enabled the ZSZ gaps to be made equal. This feature will improve the sensor characteristics such as zero output stability against temperature variation, non-linearity, and cross-talk sensitivity. The highly accurate and highly reliable three-axis accelerometer will lead to increased safety of automobiles and may enable new control methods for robots.

## References

(1) Shoji, Y., Yosida, M., Minami, K. and Esashi, M., " Diode Integrated Capacitive Accelerometer with Reduced Structural Distortion", *Proc. of Transducers '95* (1995), pp. 581-584.

(2) van Kampen, R. P., Vellekoop, M. J., Sarro, P. M. and Wolffenbuttel, R. F., "Application of Electrostatic Feedback to Critical Damping of an Integrated Silicon Capacitive Accelerometer", *Proc. of Transducers '93* (1993), pp. 818-821.

(3) Sun, C. M., Tsai, M. H. and Fang, W., "Design and Implementation of a Novel CMOS-MEMS Single Proof-mass Tri-axis Accelerometer", *Proc. of MEMS 2009* (2009), pp. 809-812.

(4) Nonomura, Y. et al., "SOI Rate Gyro Sensor for Automotive Control", *Sensors and Actuators A: Physical*, Vol. 132, No. 1 (2006), pp. 42-46.

(5) Tomonari, S. et al., "Fabrication of Silicon 3D Structure with the Cavity between a Beam and a Seismic Mass", *Proc. of Transducers '99* (1999), 2A2.3.

(6) Watanabe, Y. et al., "SOI Micromachined 5-axis Motion Sensor Using Resonant Electrostatic Drive and Non-resonant Capacitive Detection Mode", *Proc. of Transducers '05* (2005), pp. 511-514.

**Motohiro Fujiyoshi**
Research Field:
- MEMS Sensor

Academic Degree: Dr.Eng.
Academic Societies:
- IEEE
- The Institute of Electrical Engineers of Japan

**Yutaka Nonomura**
Research Fields:
- Sensors for Automobiles
- MEMS (Micro Electro Mechanical Systems)

Academic Degree: Dr.Eng.
Academic Societies:
- The Magnetics Society of Japan
- The Japan Society of Applied Physics
- The Institute of Electrical Engineers of Japan
- IEEE

Award:
- Outstanding Paper Award, Transducers, 2011

**Hirofumi Funabashi**
Research Field:
- Sensors for Automobile and MEMS Technology

Academic Society:
- The Institute of Electrical Engineers of Japan

**Yoshiteru Omura**
Research Field:
- MEMS Sensor

Academic Society:
- The Institute of Electrical Engineers of Japan

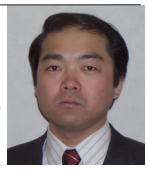

**Teruhisa Akashi**
Research Fields:
- Development of Inertial MEMS Sensors
- Mirror Devices
- Elemental Technologies Based on MEMS Fabrication Processes

Academic Societies:
- The Institute of Electrical Engineers of Japan
- The Japan Society for Precision Engineering

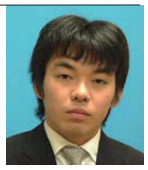

**Yoshiyuki Hata**
Research Field:
- MEMS Device

Academic Degree: Dr.Sci.
Academic Society:
- The Robotics Society of Japan

**Masayoshi Esashi***
Research Fields:
- Electronic Device/Electronic Equipment (Sensor)
- Measurement Engineering (Electronic Measurements)
- Biomedical Engineering/Biological Material Studies

Academic Degree: Ph.D.
Academic Societies:
- The Institute of Electrical Engineers of Japan
- The Japan Society of Applied Physics

Awards:
- Japan IBM Scientist Award, 1993
- SSDM Award, International Conference on Solid State Devices and Materials, 2001
- JSAP Outstanding Paper Award, The Japan Society of Applied Physics, 2005

* Advanced Institute for Materials Research, Tohoku University